ESTIMATION OF SUBSURFACE STRUCTURE BASED ON MICROTREMOR OBSERVATIONS AT PADANG, INDONESIA

Junji Kiyono [1], Yusuke Ono [2], Atsushi Sato [3], Tatsuya Noguchi [4], and Rusnardi Rahmat Putra [5]

[1] Department of Urban Management, Kyoto University, Katsura Campus, Kyoto, Japan, Tel: +81-75-383-3249, e-mail: kiyono.junji.5x@kyoto-u.ac.jp
[2] Department of Civil Engineering, Tottori University, Tottori, Japan, e-mail:ysk@cv.tottori-u.ac.jp
[3] Department of Urban Management, Kyoto University, Katsura Campus, Kyoto, Japan, e-mail: sato@quake2.kuciv.kyoto-u.ac.jp
[4] Department of Civil Engineering, Tottori University, Tottori, Japan, e-mail: noguchit@cv.tottori-u.ac.jp
[5] Department of Urban Management, Kyoto University, Katsura Campus, Kyoto, Japan, e-mail: rusnardi.rahmat@gmail.com

Received Date: January 13, 2011

Abstract

In this study, we estimated a ground profile in Padang City, Indonesia, using microtremor observations. Indonesian is located on the boundaries of three major tectonic plates, namely the Indian-Australian, Pacific, and Eurasian plates. Consequently, subduction-related major earthquakes occur repeatedly, including, even in the 21st century, such large inter-plate earthquakes as the 2004 Sumatra earthquake, the 2006 Nias Island earthquake, the 2007 Bengkulu earthquake, and the 2010 Mentawai earthquake. The 2009 Padang earthquake was also one of the most destructive earthquakes in recent times, although it was an intra-plate based earthquake. This earthquake was of magnitude Mw7.6, producing severe tremors and causing extensive damage to buildings and casualties. To prevent loss of human lives and dwellings from a devastating earthquake, we investigated the shaking characteristics of the ground in Padang. Spectral ratios for horizontal and vertical motion, H/V, from single-station microtremor records were used to identify the predominant periods of the ground vibrations. Microtremor array observations were conducted to find the phase velocities of the Rayleigh wave. The ground profile was estimated by means of the dispersion curves obtained using the Spatial Autocorrelatio (SPAC) and Centerless Circular Array (CCA) methods. The Particle Swarm Optimization (PSO) technique was introduced to determine the dispersion curves. By compiling the soil profile model obtained at each site, a three-layered generalized model was proposed. The velocity of the first layer was less than V_S = 300 m/s, the second layer V_S = 300-3000 m/s and the third layer more than V_S = 3,000 m/s. The subsurface structure models constructed provide useful information for 2-D and 3-D simulations of ground motion in Padang.

Keywords: Dispersion curve, H/V spectral ratio, Microtremor observation, Particle swarm optimization (PSO), Subsurface structure, The 2009 Padang earthquake

Introduction

The Eurasian Plate is subducting under the Indo-Australian plate off the Sumatra Island; therefore, huge earthquakes of the plate boundary type occur repeatedly every 100 to 150 years. In recent times, large destructive earthquakes occurred in 2004, 2005, 2007 and 2010 along the Sumatra trough, for which the moment magnitudes were Mw9.1, 8.6, 8.5 and 7.7, respectively [1]. In addition, a Mw7.6 intra-plate earthquake occurred at Padang on September 30, 2009. The epicenter was 45 km offshore from the Padang city center, resulting in extensive damage including more than 1,100 dead [2]. However, as this earthquake was not an inter-plate but an intra-plate earthquake, and the magnitude of the 2010 Mentawai earthquake was smaller than expected, the strain has not been fully released. This means that there is still the high possibility of another gigantic earthquake occurring in the near future (Figure 1). Thus, being prepared for an earthquake disaster is an urgent issue.

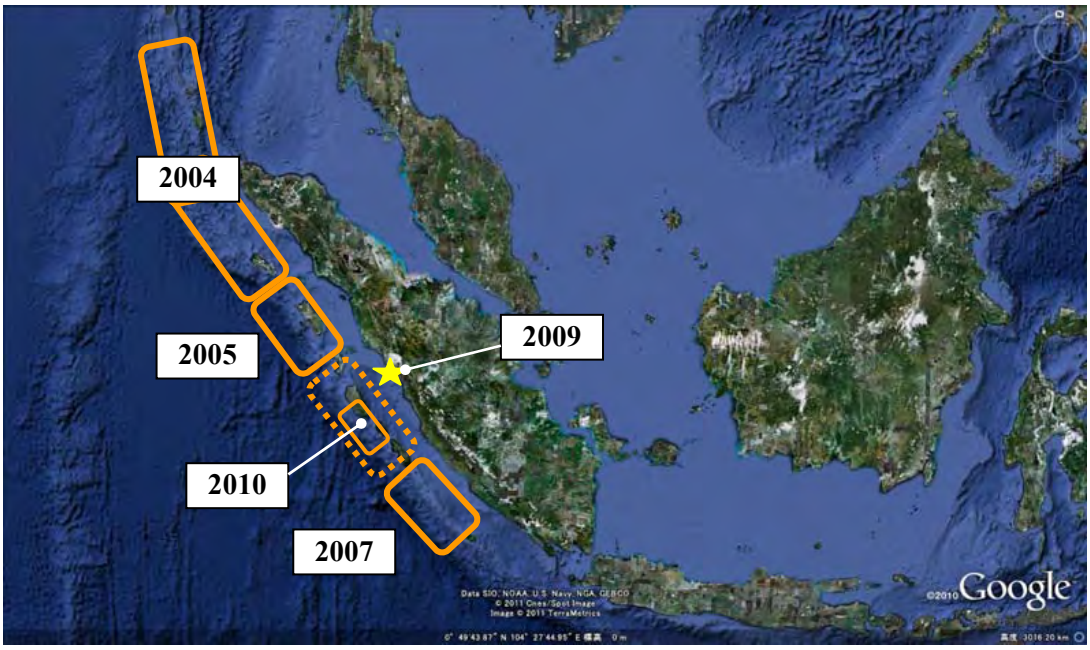

Figure 1. Recent inter-plate earthquakes between the Indian and Sunda Plates and the 2009 Padang Earthquake (drawing on Google Map)

Earthquake damage is strongly affected by site amplification from bedrock to the ground surface, as well as the size of the earthquake itself. The site amplification of the ground is controlled by factors of the sedimentary layers such as soil density, shear wave velocity, damping characteristics, shape of irregular boundaries and so on. In considering the earthquake disaster prevention measures, knowledge of the amplification characteristics and underlying structures of the ground are very important.

However there was no information about the underground profile in Padang, except for a limited amount of boring data to a depth of approximately 30 m and a subsurface geological map. In recent years, microtremor observations have become popular for the purpose of investigating soil structure, because they do not require much manpower and cost. A microtremor is a small ground vibration excited by artificial sources or natural phenomena such as factories, traffic, wind, waves, etc. As the vibration propagates through the ground surface, the surface waves such as the Rayleigh- and Love-waves are dominant.

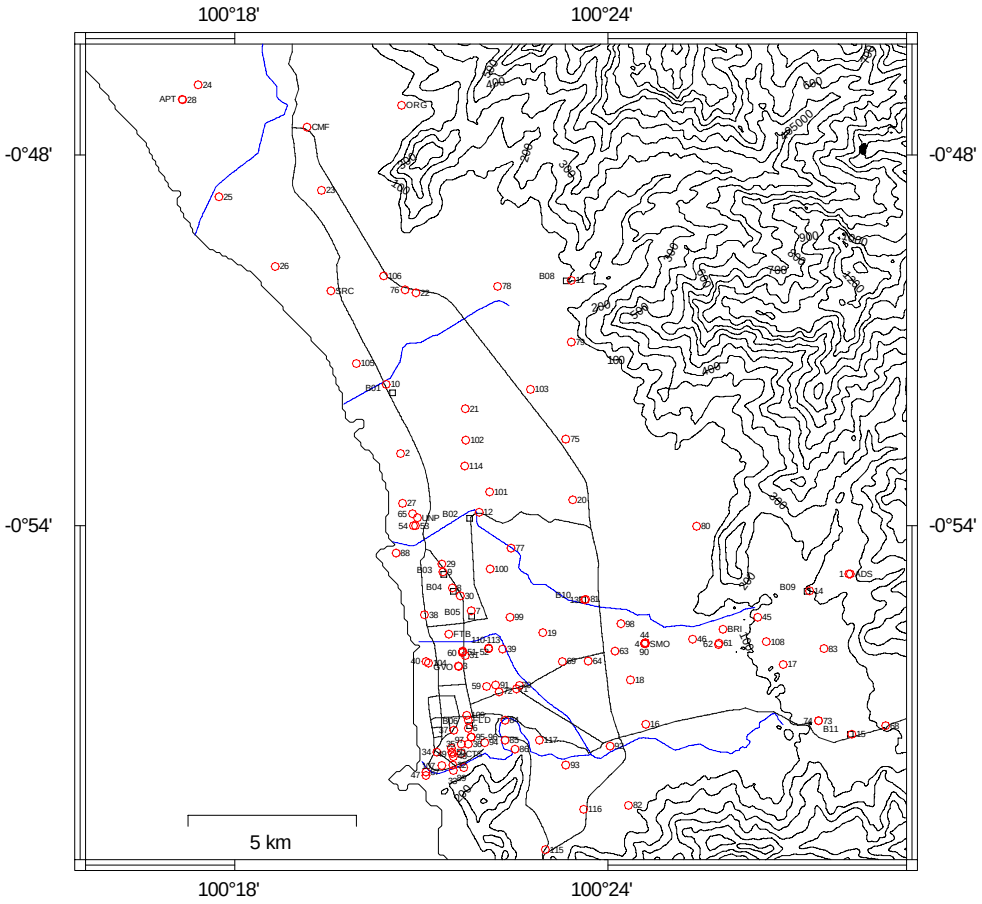

Figure 2. Location of the microtremor observation sites

Ono et al. [3] and Noguchi et al. [4] clarified during their surveys over the 2008 to 2009 period that extensive deep sedimentary layers exist for which the predominant period is about two seconds using the results of single-point observations. They also clarified through the array observations that the coastal area in Padang is covered by a surface layer 20-40 m thick, for which the shear wave velocity is around 200 m/s. Although single-point observations were conducted at point 62, higher density observations are needed to find local irregularities of the underground soil structure. As the deep soil structure of the plain is still unclear because the radius of the array was small (1-30 m), larger array observations, for which the radius is several hundred meters, are required in order to show deep ground profiles. In addition, previous studies proposed only a one-dimensional soil structure directly beneath the site, therefore, the extension of the soil structure model to two- or three-dimensional space is highly desirable.

In this study, Padang, where a large earthquake is expected in the near future, is considered to be a target area. We carried out higher density single-point observations and larger radius array observations. Based on the observed data, we calculated the distribution of the predominant and phase velocities of the Rayleigh wave. Finally, we constructed a 3-dimensional subsurface structure of the sediment in Padang.

Microtremor Observations

A three-component accelerometer with data logger, GPL-6A3P, produced by the Akashi Co. Ltd., was used. Observations were done in the daytime at places away from noise

sources such as vehicle traffic and which provided stable conditions for the installed equipment such as a concrete or asphalt base. The number of single-point observations was 129. The sampling frequencies were 100 Hz or 500 Hz and the observation times were 10 to 15 minutes. Array observations were carried out at 11 sites with sampling frequencies of 100 Hz or 500 Hz, and observation times of 20 to 30 minutes. The overall observation sites are shown in Figure 2.

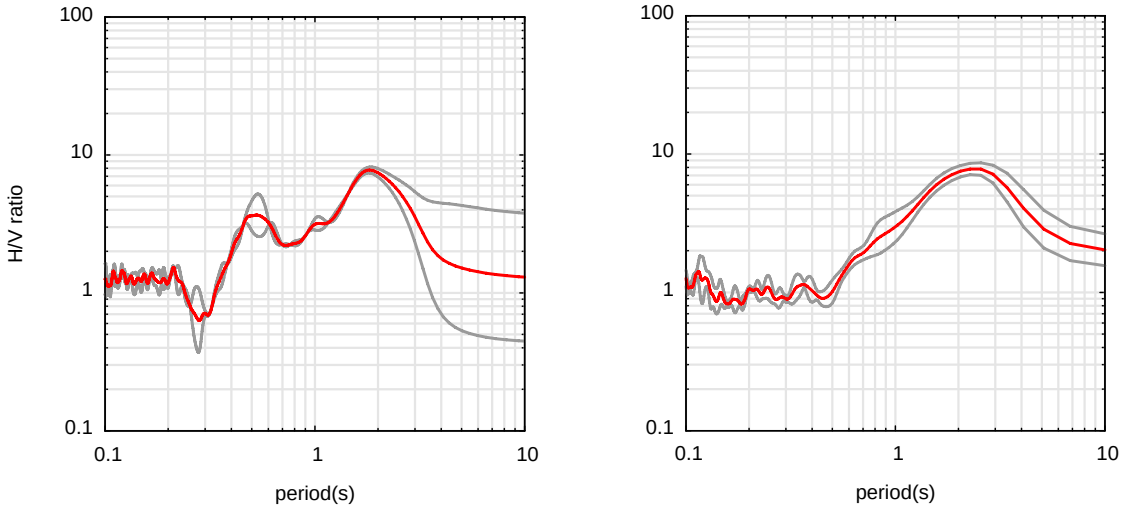

(a) two distinct peaks (b) single clear peak

Figure 3. Example of the H/V spectrum ratio (mean value and 1 deviation)

Predominant Period of H/V Spectra

The spectral ratio of horizontal and vertical motion obtained by microtremor observations is called the H/V spectrum. The predominant period of an H/V spectrum is thought to be equivalent to the predominant period of the ground directly beneath the site. H/V spectra at each site in the target area were calculated. We classified the H/V spectra calculated into three types according to the shape of the spectra.

- ✓ Type A: those with two distinct peaks (Figure 3(a))
- ✓ Type B: those with a single clear peak (Figure 3(b))
- ✓ Type C: those without clear peaks

Distinct peaks express the characteristics of the layers for which the shear wave velocity is quite different. According to this interpretation, the lower and higher periods in Type A represent the effects from deep and shallow soil layers, respectively. In Type B, the difference between the two layers is not marked, and the effect of one layer is absorbed into that of the other layer. Type C is an observation site that has hard soil or did not work well. Thus, we established the data for both long and short predominant periods, T_d and T_s. Although the predominant period does not always indicate the characteristics of an individual layer because typically the actual shaking mode of the ground is complex, we assumed that the long and short periods reflected information from each layer.

Although there are 129 observation points, the points are not adequate to cover all the target area. If each value of the predominant period obtained is considered to be a

realization of a stochastic random field, we can use the Kriging technique [5], which is one of the interpolation techniques that considers the covariance of the random field.

From the distribution of the predominant period, T_d, which expresses the information for the deep sedimentary layer, we found a deep layer with a period of two to three seconds extending in the plain along the coast. In the vicinity of CTS and SMO in south Padang, a rapid change in the predominant period can be seen. This means an abrupt change has occurred in the interface of the underground soil. The short predominant period, T_s, which reflects the information of relatively shallow soil layer, is around 0.6 s in the plain area and becomes shorter with an increase in altitude. The spatial distributions of shorter- and longer-predominant periods are shown in Figure 4(a) and (b).

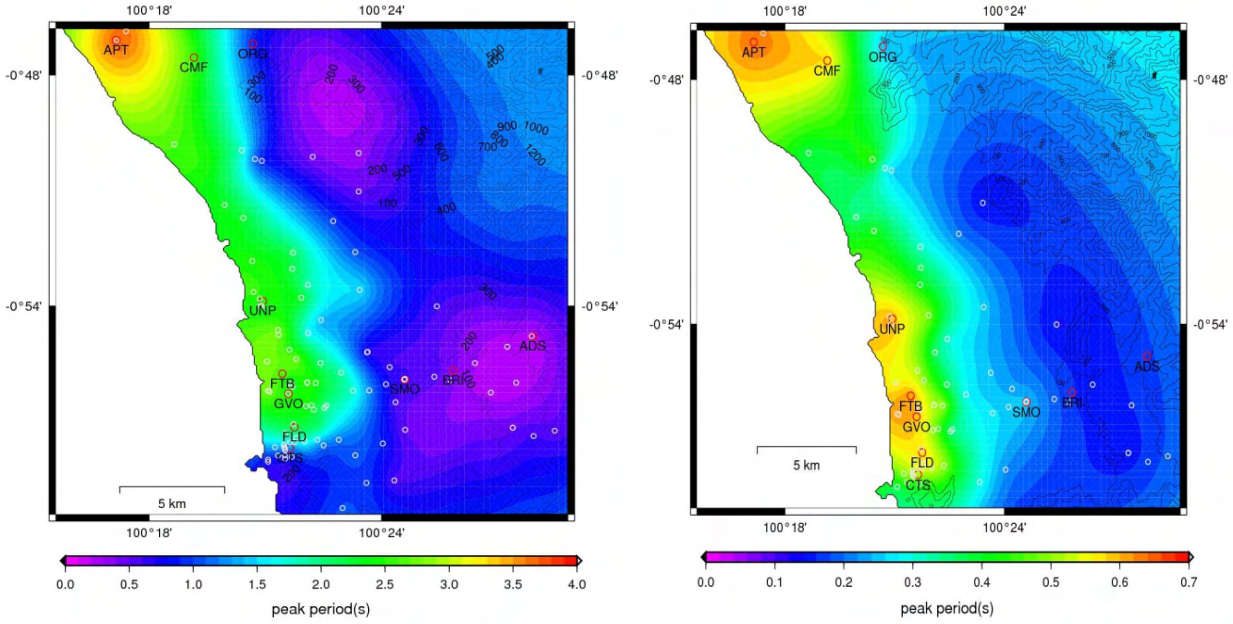

(a) T_d (b) T_s

Figure 4. Spatial distributions of longer and shorter predominant periods, T_d and T_s

Dispersion Curves by Array Observation

Array observations provide simultaneous observations from several instruments appropriately arranged. The phase velocity of the surface wave can be estimated using these synchronized recordings. The phase velocities of a Rayleigh wave propagating in a layered media show dispersion characteristics. The dispersion curve can be obtained by combining several phase velocity curves estimated from different array radii. The aim of the array observation is to determine the soil profile beneath the site by inverting the dispersion curve.

In this study, we adopt the SPAC [6] and CCA [7] methods. SPAC is a method by which the phase velocity is calculated for every frequency from the Bessel function argument by averaging the normalized coherence function defined as the spectrum from a site pair on the array. On the other hand, CCA is a method by which the wave number of a Rayleigh wave is calculated for every circular frequency by taking the ratio of the power spectra of the zero- and first-order Fourier coefficients averaged along the array circle.

The CCA method does not need an array with a large radius, and can be applied to wavelengths ten times larger than the array radius. Therefore, we calculated the dispersion curves by both the traditional and new methods, and depict the dispersion curve by choosing the dispersion from the lower frequency side.

Array observations were carried out at 11 sites along the three survey lines (lines A, B and C) as shown in Figure 5.

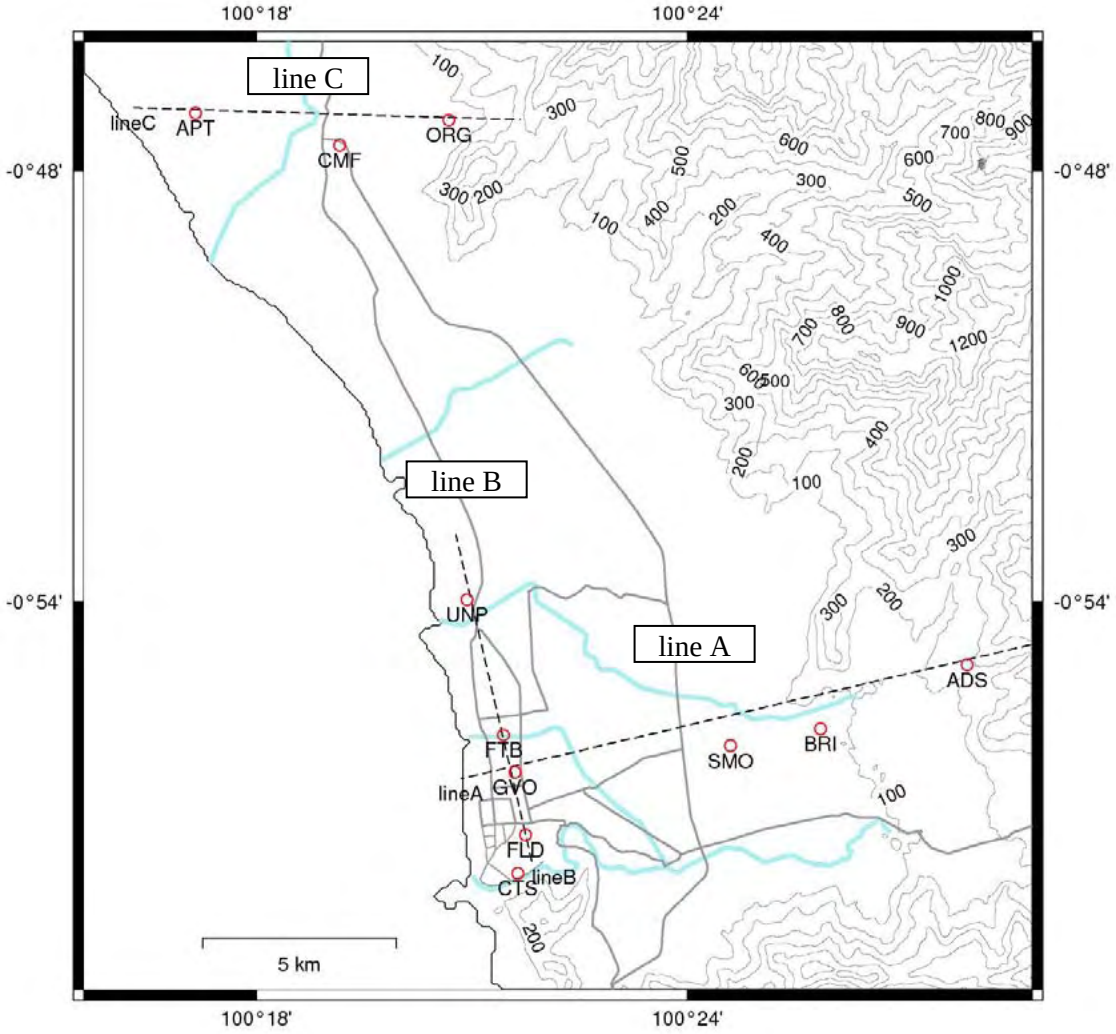

Figure 5. Three Survey Lines for Array Observations (line A, line B, and line C)

The dispersion curves obtained are shown in Figure 6(a), (b) and (c) for each survey line with altitude (d). For line A, the phase velocity corresponding to shallow ground with a high frequency range is about 200 m/s at GVO, about 400 m/s at SMO, about 500 m/s at BRI and about 300 m/s at ADS. The soft ground extended beneath GVO, which is the nearest site to the coast. The ground beneath the sites higher than SMO has relatively hard surface soil compared with the plain along the coast. As a whole, there is a larger difference in subsurface structure between GVO and the other sites, SMO, BRI and ADS, judging from the minimum value of the high-frequency phase velocity, and the frequencies showing the dispersion characteristics. For line B, dispersion characteristics were observed at all sites in the frequency range lower than 5 Hz, and all the shapes had the same tendency. Since the minimum phase velocity in the high frequency range is around 200 m/s,

the soil profile is very similar along line B. For line C, the curves at CMF and APT are almost identical and the minimum phase velocity is 150 m/s; however, the curve for ORG has a different shape for which the minimum phase velocity is 350 m/s.

The dispersion curves obtained here had no discrepancies in the distribution of topography, altitude and predominant period. We could estimate subsurface sedimentary layers in the plains using these dispersion curves.

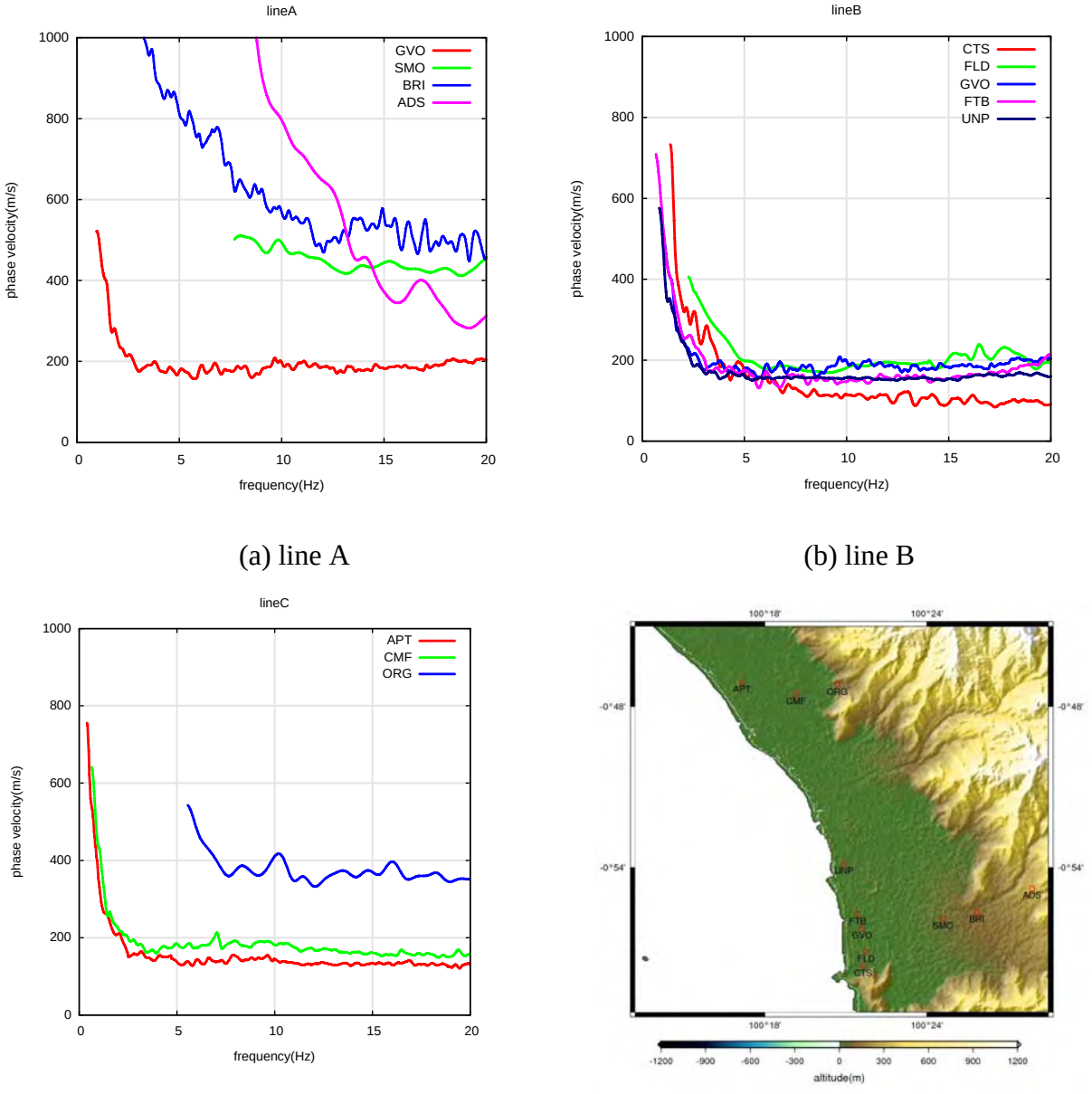

(a) line A (b) line B

(c) line C (d) altitude map

Figure 6. Dispersion curves obtained for each survey line

Estimation of V_s Structure by Inversion

Application of PSO

By conducting an inversion analysis using the Particle Swarm Optimization (PSO) algorithm on the above dispersion curves, the subsurface structure beneath the site can be

estimated. The PSO is a solution method for a non-linear optimization problem [8]. We estimate the subsurface structure of the model by minimizing the difference between the observed and theoretical phase velocity curves.

$$F = \sum_{i=1}^{N} w_i \sqrt{(c_i^o)^2 - (c_i^T)^2} \tag{1}$$

where F is an objective function that should be minimized, c_i^O and c_i^T are the observed and theoretical phase velocities, and w_i is a weighting function. c_i^O and c_i^T are given in discretized frequency ($i=1, 2, \ldots, N$). The PSO uses a particle swarm that has information about position and velocity. The particle swarm moves around the space with updating information and settles at the optimized point. During the optimization, the particle swarm has a best solution for both the group (g-best) and individual particle (p-best) in every step. The basic procedure of PSO is as follows.

After setting the initial values of the number of particles and iterations, an initial position and velocity are given to x_d^k and v_d^k, in which d is a particle number. The value of the objective function is calculated for each particle. The best solutions for the particle, d, and for the group, g, at k-th iteration are defined as p_d^k and p_g^k. Then the position and velocity are updated as

$$v_d^{k+1} = w v_d^k + c_1 r_1 (p_d^k - x_d^k) + c_2 r_2 (p_g^k - x_g^k) \tag{2}$$

$$x_d^{k+1} = x_d^k + v_d^{k+1} \tag{3}$$

where r_1 and r_2 are random values with the range of [0, 1], c_1 and c_2 are constants, and w is the inertia weighting. This process is repeated as $k=k+1$ until the number of iterations exceed a setting value.

Before performing the inversion analysis, the subsurface structure was assumed to consist of horizontal layers of elastic and homogeneous medium upon a semi-infinite elastic body. The shear wave velocity and thickness of each layer are the parameters that were determined by inversion analysis. The results obtained enable us to determine the soil condition of the subsurface structure [3].

For the sites on the plain with a thick sediment (CTS, FLD, GVO, FTB, UNP, CMF, APT), the information about the phase velocity for the long period dispersion curves is inadequate; therefore, the results are insufficient to make the observed and theoretical dispersion curves coincide. In this study, we considered another criterion in which the peaks of both the observed and theoretical H/V spectrum match each other as much as possible, in addition to the compatibility of the dispersion curves.

The inversion process was undertaken using the following method: 1) Assuming that the media was four-layered with regular boundaries, and the density, ρ, and shear wave velocity, V_s, of the base layer were 2.4 tonf/m^3 and 3,000 m/s. The densities of the upper three layers were fixed at 1.7, 1.8, and 1.9 tonf/m^3 from the surface, respectively. The variables were the thicknesses, H_1, H_2 and H_3, and the shear wave velocities, V_{S1}, V_{S2} and V_{S3}, of the top three layers. Initial vales were decided by taking into account the observed dispersion curves, H/V spectra, and topographical characteristics such as altitude and geological conditions. 2) Reviewing the results obtained from the above procedure, for the sites that did not reflect a predominant period of H/V (probably due to a deep sediment in the plain), we repeated the inversion. Since the shape of the dispersion curve was not much

affected by the variation of the parameters for the third layer, we re-estimated the values of H_3 and V_{S3} in order to fit the predominant period for both H/V spectra.

An example of the identified soil parameters by the inversion at GVO is shown in Table 1. Figures 7 (a) and (b) show dispersion curves and H/V spectra at GVO. The observed and theoretical dispersion curves were in good agreement, and the predominant period of the improved theoretical H/V spectrum became closer to the observed one. It was found that the subsurface structure could be estimated reasonably using this proposed sequential procedure.

Table 1. Identified Ground Parameters at GVO

Layer	ρ [t/m^3]	V_p [m/s]	V_s [m/s]	H [m]
1	1.7	1003	194	42
2	1.8	1325	329	81
3	1.9	1621	479	131
4	2.4	5196	3000	-

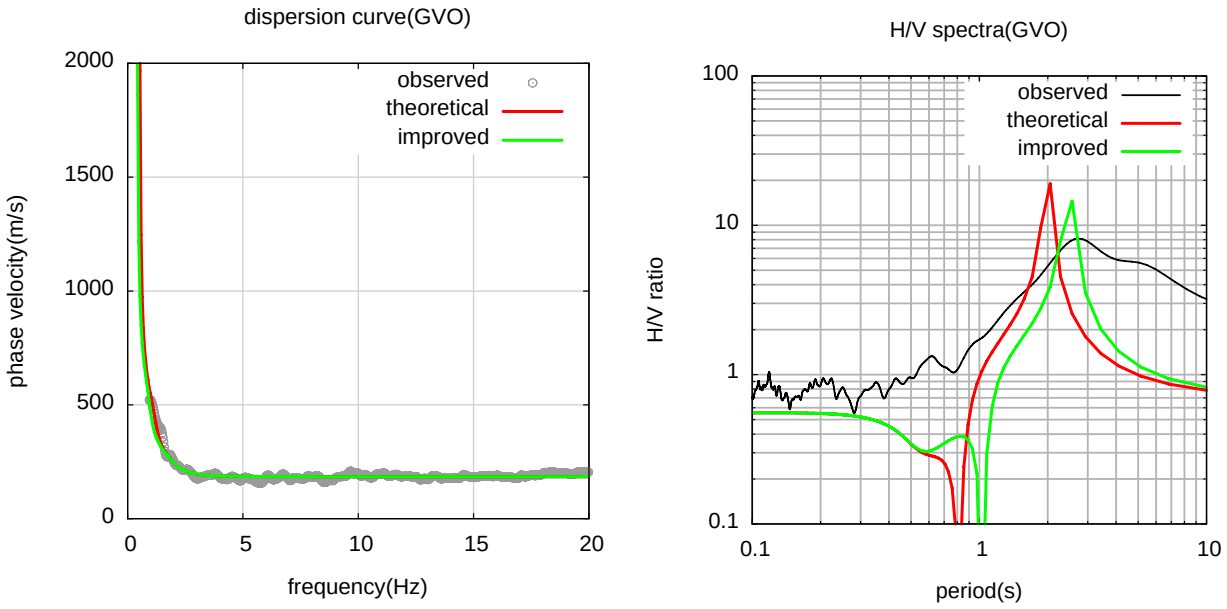

(a) dispersion curve (b) H/V spectra

Figure 7. Dispersion Curves and H/V Spectrum Ratios at GVO

Results of Inversion and Discussion

line A

The V_s structure along line A is shown in Figure 8(a). Looking at a surface layer at GVO, the thickness of the first layer with V_s = 200 m/s is about 40 m, however, the corresponding layer cannot be seen for SMO, BRI and ADS. The thickness of the sediment is about

250 m/s at GVO, on the other hand, those at SMO, BRI, ADS are 30 m, 30 m and 10 m, respectively. As seen in the distribution of the predominant period of the H/V spectra, we can also guess at the existence of a rapid change in the subsurface structure between GVO and SMO.

line B

The V_s structure along line B is shown in Figure 8(b). For all the sites, the velocities of the first, second, and third layers are 200 m/s, 350 m/s and 500 m/s. The thickness of the first layer is around 20 m to 40 m. The sediment thickness is about 250 m and almost uniform. This tendency is in good agreement with the results of the predominant period distribution characteristics.

line C

The V_s structure along line B is shown in Figure 8(c). At the sites in the plain, CMF and APT, the thickness of the layer with V_s = 150 m/s is around 30 m to 70 m, but the layer disappeared at the site near the mountain, ORG. The sedimentary thickness is almost constant, 250 m, at APT and CMF but is shallow at ORG.

Although we could construct a four-layered model for each line, it is still difficult to compile all the information because some layers of a site cannot connect to those of other sites; therefore, a three-layered model is introduced as an alternative.

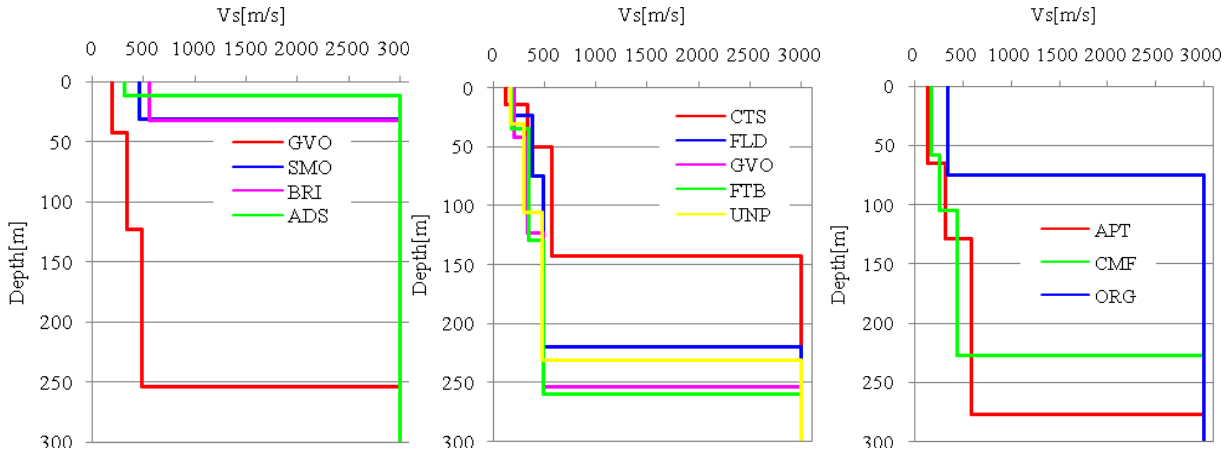

(a) line A (b) line B (c) line C

Figure 8. V_s Structure of the ground along the survey lines

Modeling of Subsurface Structure in Padang

H/V Spectra of Shallow Ground

According to the inversion analysis discussed above, the peak of the H/V spectrum in the long period part at the sites in the plain area, CTS, FLD, FTB, GVO, UNP, CMF, could be explained by the theoretical ground model. To verify if the peak of the H/V spectrum in the short period part could be explained by the theoretical ground model, we made a shallow ground model at CTS composed of surface and semi-infinite layers. The soil parameters assumed are shown in Table 2. The theoretical and observed H/V spectra are shown in Figure 9. The theoretical H/V approximately defined the peak of the short period part. The actual predominant periods of the layer media, of course, did not always correspond to the

natural period of each layer because the behavior of a multi d-o-f system is described by the superposition of individual modes. However, where the number of layers is small and impedance ratios are large, the above approximation is reasonable.

Table 2. Ground Parameters Estimated for the Verification of Short-period Peak (CTS)

layer	ρ [t/m^3]	V_p [m/s]	V_s [m/s]	H [m]
1	1.7	778	118	142
2	1.8	1327	331	-

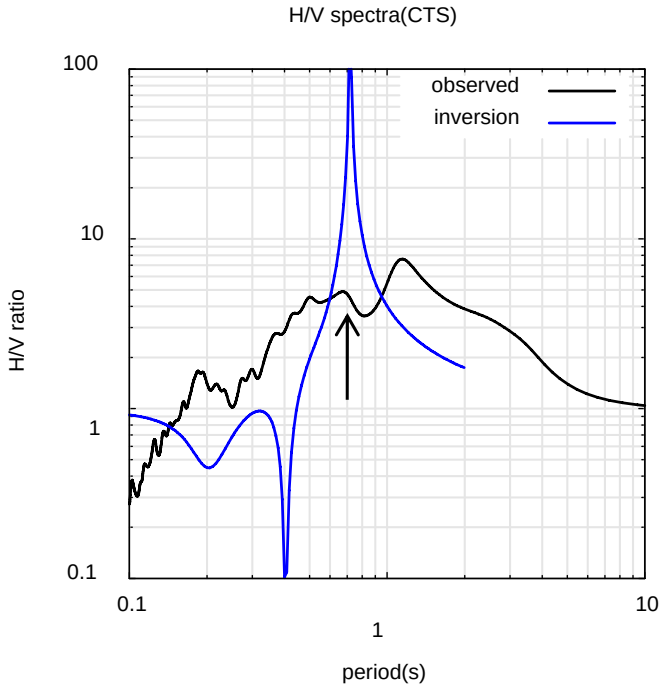

Figure 9. Comparison between theoretical and observed H/V spectra

Determination of Layer Thickness

The peaks in the short and long periods of the observed H/V spectrum could be explained by the estimated subsurface soil structure. In this study, we used the two distinct peaks in the observed H/V spectra and V_s structure obtained by array observation. The technique used was the 1/4 wavelength principle, which can approximately be extended to multi-layered media.

$$T = 4H / V_S \tag{4}$$

where H is a thickness of a layer. Here we divided the ground into three layers; the upper two layers and a base semi-infinite layer. The range of the shear wave velocity for the first, second and third layers is assumed (I) $V_s \leqq$ 300 m/s, (II) 300 < V_s <3000 m/s and (III) $V_s \geqq$ 3000 m/s.

The target area is shown in Figure 10, in which the rapidly varying area of the subsurface condition and dense observation area are enclosed.

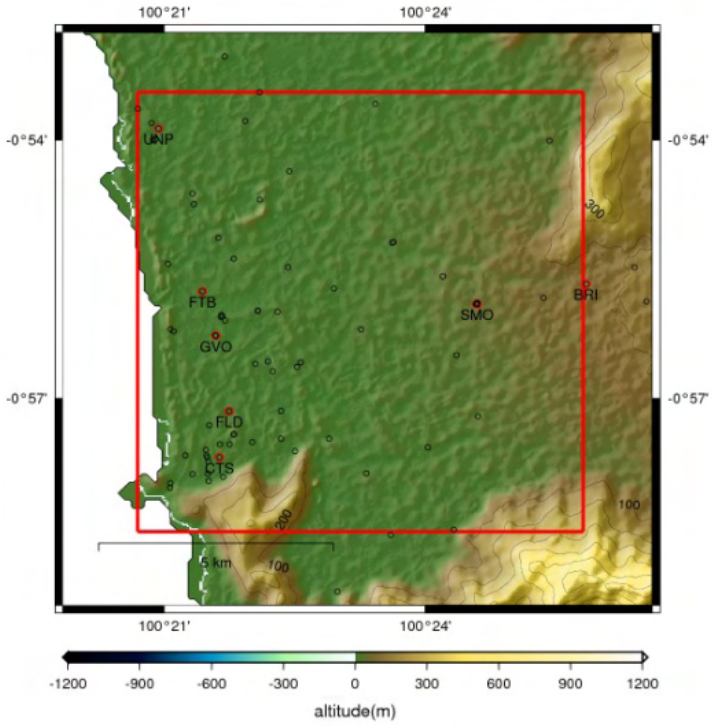

Figure 10. Target area for the analysis of three-layered model

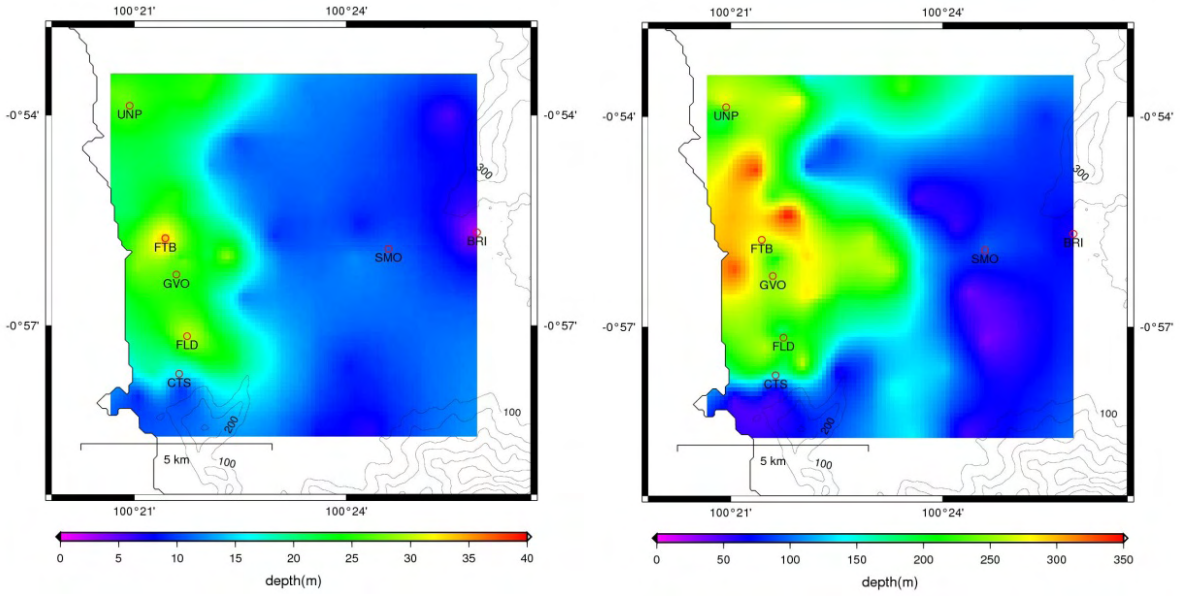

(a) depth of layer-I (b) depth of layer II

Figure 11. Depth of the boundaries between layer-I, II and III in 2D

The ground model is constructed as follows: The rectangular area (about 10 km*10 km) in Figure 10 is divided into100*100 meshes (100 m square). According to the Kriging technique, the values of predominant periods, T_s and T_d, at the center of each mesh are interpolated by using the finite number of peak periods read from the observed H/V spectrum.

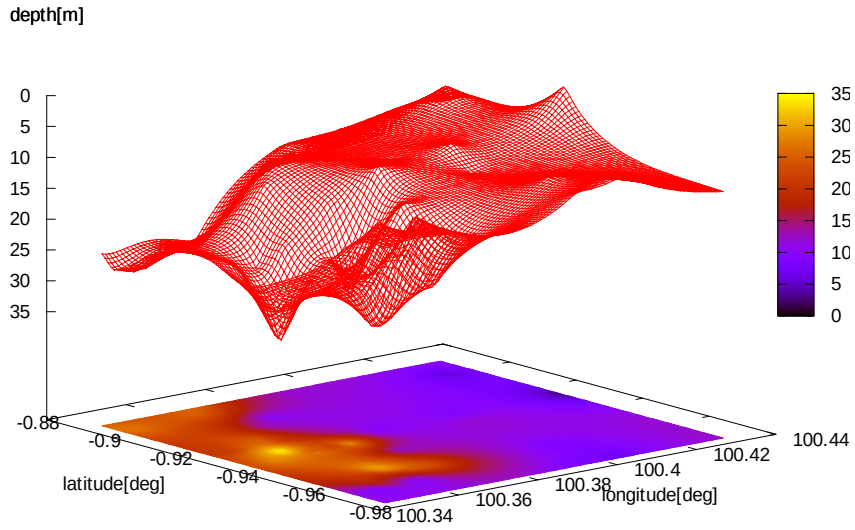

(a) boundary depth between the first and the second layer

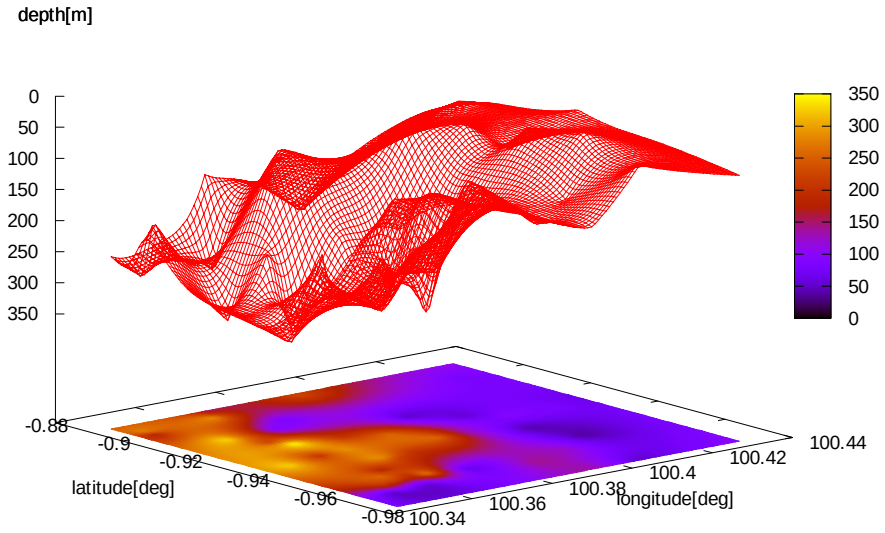

(b) boundary depth between the second and the third layer

Figure 12. Three-dimensional shape of the estimated subsurface structure

The shear wave velocities, V_S*, of layer-I and layer-II are calculated by the weighted average, for which the weight is the reciprocal of square of distance from the array observation points, GVO, SMO, BRI, CTS, FLD, FTB and UNP, as

$$V_S^* = \frac{\sum_{i=1}^{7} V_{Si} / x_i^2}{\sum_{i=1}^{7} 1 / x_i^2} \tag{5}$$

where i defines the array site ($i=1,2,\ldots,7$), and x_i indicates the distance between an array observation site and the center of the mesh.

Using the interpolated shear wave velocities of layer-I and layer-II, and the predominant periods, T_s and T_d, we derive the depth of the first and second layers of the sediment as shown in Figures 11(a) and (b).

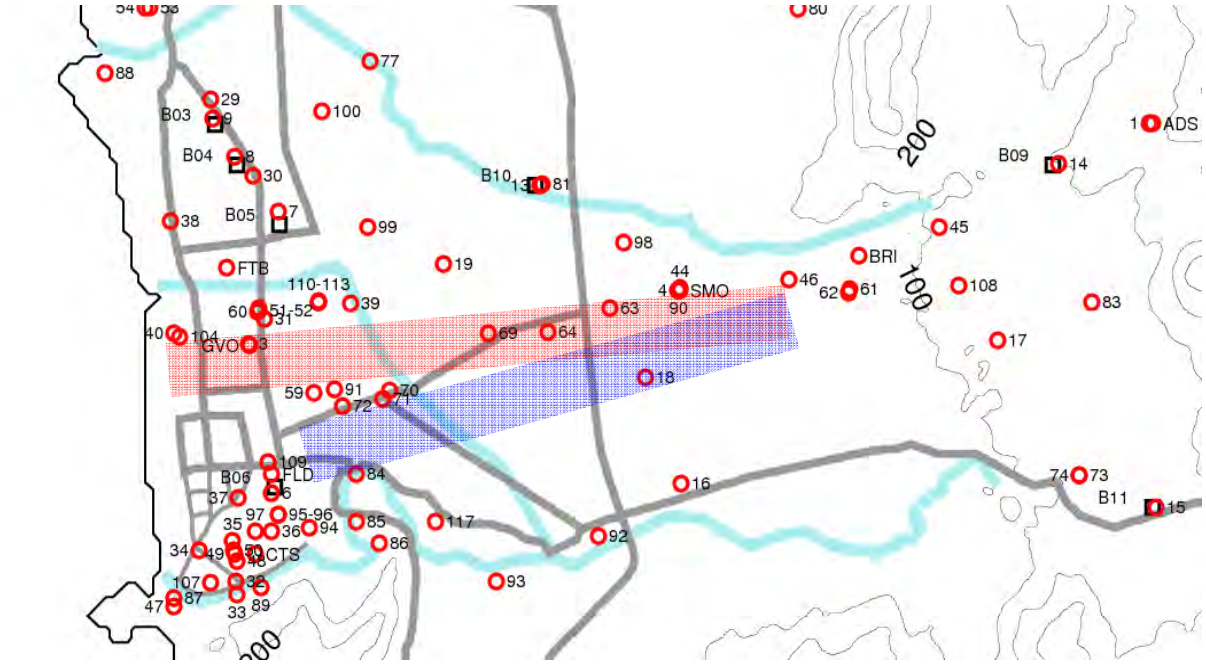

Figure 13. Two lines for the investigation of the period change near SMO

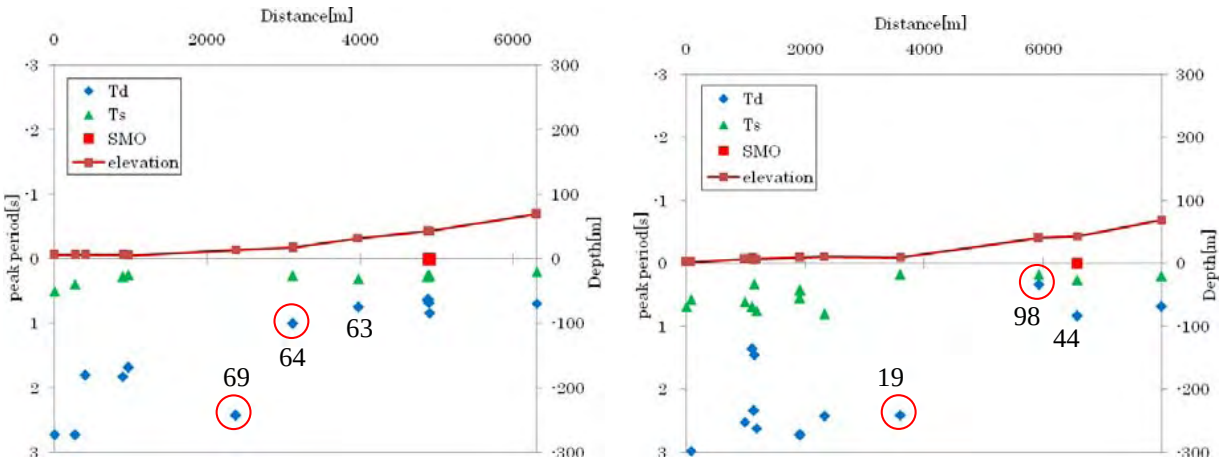

(a) along the lower line in Figure 13 (blue line) (b) along upper-line in Figure 13 (red line)

Figure 14. Variation of peak values for the predominant period along the two lines

Modeling of the Three-dimensional Subsurface Structure

Figure 12(a) shows the boundary depth between the first and second layers plotted in 2D and 3D form. Around a 30 m thick layer of sediment uniformly accumulated along the coast in the plain. The sediment becomes thinner from the coast to the eastern mountains.

The boundary between the second and the third layer is shown in Figure 12(b). The boundary depth was around 250-350 m and appeared very deep. In the west of the site, SMO, the depth of the boundary drastically changed from 250-350 m to 50 m. Rapid change can also be seen in the southern part of the area near the CTS site because of the mountain location.

Focusing on the site SMO, although the elevation of surrounding area is almost at the same level, a sudden change in sedimentary layers can be seen. Here we align the predominant periods of the H/V spectra in the order of elevation along the two shaded lines (Figure 13). These are shown in Figures 14(a) and (b), in which the lower and upper lines in Figure 13 correspond to Figures 14(a) and (b), respectively. In Figure 14(a), a large gap of 1.5 s appears between sites 64 and 69, for which the distance is very small. A similar gap of 2.0 s can be found between sites 109 and 98 in Figure 14(b). The cause of the large gap in the narrow area is the existence of a fault, which can be often be found in a sedimentary plain.

At present, since there are no detailed ground survey data in Padang such as deep boring, gravity anomalies, and seismic exploration, the existence of a hidden fault is just an estimation from microtremor observations. However, if a hidden fault exists beneath Padang City, we should prepare for a near-source earthquake here in Padang. For future work, additional dense array observations combined with other ground survey techniques need to be done to clarify the detailed subsurface structure, especially around the SMO site.

Conclusions

Our observations and analyses provide useful and practical data for earthquake disaster mitigation in Padang. The procedure employed and conclusions obtained in this study are as follows.

1) Microtremor observations were carried out for constructing a subsurface ground model in Padang. Single-point observations and array observations were conducted at 129 and 11 sites respectively, which covered almost the whole city area.
2) H/V spectra were calculated at all the single-observation sites and a distribution of predominant periods was obtained. Basically the spectrum had two peaks, each of which reflects the information of a shallow and a deep layer. The dispersion curves of a Rayleigh wave were obtained from the data of array observations.
3) The Kriging method can be used for the interpolation of subsurface information such as predominant period, shear wave velocity and depth of irregular boundary.
4) By conducting an inversion analysis for the calculation of dispersion curves, the subsurface structure beneath the site can be estimated. The Particle Swarm Optimization (PSO) algorithm was adopted for the inversion analysis. PSO is a simple but useful tool for optimization.
5) We constructed a three-layered model for making a three-dimensional structure, for which the shear wave velocities were (I) $V_s \leqq 300$ m/s, (II) $300 < V_s < 3000$ m/s and (III) $V_s \geqq 3000$ m/s. Around a 30 m thick sedimentary layer with $V_s \leqq 300$ m/s uniformly

accumulated along the coast in the plain. The sediment became thinner from the coast to the mountain. The boundary depth between the second and the third layer was around 250 m to 350 m with 300 $< V_s <$3000 m/s.
6) A sudden change in sedimentary layers could be seen near the SMO site. This might be a hidden fault, therefore, other ground surveys such as a deep boring, gravity anomaly, or seismic exploration need to be done to clarify the detailed subsurface structure and to mitigate future damage.

Acknowledgements

This study was supported by the JICA-JST Project "Multi-disciplinary Hazard Reduction from Earthquake and Volcanoes in Indonesia" (Project leader: Prof. Kenji Satake, ERI, University of Tokyo), and in part by the Global COE Project "Global Center of Education and Research on Human Security Engineering for Asian Megacities" (Project leader: Prof. Yuzuru Matsuoka, Kyoto University). We gratefully acknowledge Dr. Abdul Hakam, School of Civil Engineering, Andalas University, for his cooperation with the microtremor observations. We sincerely thank Mr. Masaaki Kubo, Mr. Tatsuki Ikeda and Mr.Takuji Horio, ex-students at Kyoto and Tottori Universities, for their help in undertaking the observations in Padang, Indonesia.

References

[1] R.R. Putra, J. Kiyono, and Y. Ono, "Seismic hazard Analysis for Indonesia," In: *Proceedings of International Symposium on a Robust and Resilient Society against Natural Hazards and Environmental Disasters and the Third AUN/SEED-Net Regional Conference on Geo-Disaster Mitigation*, Kyoto, Japan, pp. 55-61, 2010.

[2] Indonesian National Board for Disaster Management (BNPB), *Total Damage Report and Verification for West Sumatra due to Padang Earthquake*, BNPB report, 2009: Author.

[3] Y. Ono, J. Kiyono, P.R. Rusnardi, and T. Noguchi, "Microtremor observation in Padang city, Indonesia to estimate site amplification of seismic ground motion," In: *Proceedings of International Symposium on a Robust and Resilient Society against Natural Hazards and Environmental Disasters and the Third AUN/SEED-Net Regional Conference on Geo-Disaster Mitigation*, Kyoto, Japan, pp. 386-391, 2010.

[4] T. Noguchi, T. Horio, M. Kubo, Y. Ono, J. Kiyono, T. Ikeda, and P.R. Rusnardi, *Estimation of Subsurface Structure in Padang, Indonesia by Using Microtremor Observation*, Report on Earthquake Disaster Prevention Field Sequence No. 26, Tono Research Institute of Earthquake Science, pp. 1-16, 2009. (in Japanese)

[5] J. Kiyono, and M. Suzuki, "Conditional simulation of stochastic waves by using Kalman filter and kriging techniques," In: *Proceedings of the 11th World Conference on Earthquake Engineering*, Elsevier Science Ltd., Acapulco, Mexico, Paper No. 1620, 1996.

[6] K. Aki, "Space and time spectra of stationary stochastic waves, with special referent to microtremor," *Bulletin of Earthquake Research Institute*, Vol. 35, No. 3, pp. 415-456, 1957.

[7] I. Cho, T. Tada, and Y. Shinozaki, "A new method to determine phase velocities of Rayleigh waves from microseisms," *Geophysics*, Vol. 69, No. 6, pp. 1535-1551, 2004.

[8] J. Keneddy, and R.C. Eberhart, "Particle swarm optimization," In: *Proceedings of IEEE International Conference on Neural Networks*, Vol. 4, Institute of Electrical and Electronics Engineers (IEEE), Perth, Western Australia, Australia, pp. 1942-1948, 1995.